Short Communication:

Precipitation, Synthesis, and Characterization of Hydroxyapatite Derived from Gonggong Snail Shells (*Strombus canurium*)

Najla Maritza[1], Beauty Suestining Diyah Dewanti[1*], and Leny Yuliatun[2]**

[1]*Department of Agroindustrial Technology, Faculty of Agriculture Technology, Brawijaya University, Jl. Veteran, Malang 65145, Indonesia*

[2]*Research Center of Biomass and Bioproduct, National Research and Innovation Agency, Soekarno Science and Technology Area (KST), Jl. Raya Jakarta-Bogor Km. 46 Cibinong, Bogor 16911, Indonesia*

* ***Corresponding author:***

email: beauty_dewanti@ub.ac.id; leny004@brin.go.id***

Received: June 5, 2025
Accepted: December 1, 2025

DOI: 10.22146/ijc.107110

Abstract: *The gonggong snail shell contains high calcium, reaching 67.70%, which potential to be used as a source of natural hydroxyapatite (Hap). The purpose of this study was to analyze the effect of temperature and precipitation synthesis time on the characteristics of HAp produced from the gonggong snail shell for bone substitute biomaterials. The results showed that precipitation at 900 °C for 4 h is the best solution for synthesizing HAp with a Ca/P ratio of 2.76, closely approximating the stoichiometric value of HAp. SEM results revealed that the synthesized HAp exhibited a spherical morphology with a tendency to form granular aggregates. FTIR confirmed the presence of characteristic PO_4^{3-} and OH^- groups. XRD analysis indicated that primary phase of the synthesized material was HAp, consistent with JCPDS data. The optimal immersion time and temperature for fabricating at 900 °C for 4 h in HAp:alginate ratio (w/w) of 2.5:7.5 (HAPT2C) based on their mechanical properties. However, HAp:alginate ratio (w/w) of 5:5 (HAPT2A) demonstrated higher water absorption compared to HAPT2C in the water uptake test. HAp from gonggong snail shell are promising biomaterial candidates for bone substitution applications, warranting further investigation through* in vitro *and* in vivo *biocompatibility studies.*

Keywords: *gonggong snail shell; hydroxyapatite; precipitation synthesis*

■ INTRODUCTION

In recent years, traffic accidents have often occurred in Indonesia. In 2022, the traffic accident rate in Indonesia reached 94,617 victims, 19,054 of whom died. In fact, the number of traffic accidents from January to September 13, 2022 increased from 2021 by 34.6% with a total of 25,266 victims. The impact of the accident causes injuries, defects or bone damage in the victim [1]. Defects or fractures in the bone can be treated using bone implants. The application of bone implants requires consideration of biocompatibility, chemical properties, mechanical properties, and surface properties of the material. The implant must have similar biomechanical properties to those of the bone and be integrated with the native tissue [2].

Bone implants can be formed using biomaterials. Biomaterials can be designed to interact with biological systems to repair and replace damaged tissues, body systems, or organs [3]. Biomaterials are obtained from natural sources or waste. Especially in Indonesia, water waste has not been optimally utilized, and most of it is simply discharged into the environment, causing environmental problems such as disturbing public comfort, contributing to environmental pollution, and leading to various diseases. This happened on Bintan Island in the Riau Islands where there was an accumulation of gonggong snail shell waste (*Strombus canurium*) [4].

The shell of the gonggong snail contains high calcium, reaching 55.51%, with the remaining content

being iron, aluminum, and potassium. This abundant calcium content has the potential to be used as a source of natural hydroxyapatite (HAp) [5]. HAp with the chemical formula $Ca_{10}(PO_4)_6(OH)_2$ is a calcium phosphate compound that is the main inorganic component in the structure of teeth and bones [6]. HAp has a crystal form in body fluids and resembles minerals in bones. The HAp content can be used as a biomaterial for bone substitutes or biomedical scaffolds because it is able to integrate with bone tissue without causing toxic effects or inflammation [7]. HAp has superior biocompatibility and bioactivity properties. HAp's biocompatibility properties show its ability to increase corrosion resistance while improving implant compatibility with the body. Meanwhile, HAp's good bioactivity allows this material to be a place that supports the growth of new bone tissue. HAp has a molar ratio between calcium and phosphate (Ca/P) of 1.67, which is close to the molar ratio in bone tissue. Therefore, HAp has been widely applied in the biomedical world [8].

One of the methods used in HAp synthesis is precipitation. The precipitation synthesis process involves the addition of phosphate groups to a suspension containing calcium ions. In this reaction, HAp is synthesized using two types of precursors, namely orthophosphoric acid (H_3PO_4) and calcium hydroxide ($Ca(OH)_2$). The use of these two precursors aims to reduce the risk of HAp synthesis failure while increasing the efficiency of the synthesis process [9]. The precipitation method has the ability to produce HAp with high yields while providing ease in modifying the particle surface. This method is also known to be simpler and more economical, making it suitable for application on an industrial scale [10]. In addition, the microstructure of HAp produced by the wet chemical precipitation method has a higher similarity to natural bone minerals compared to the sol-gel method [5]. The purpose of this study was to analyze the effect of temperature and synthesis time on the characteristics of HAp produced from gonggong snail shells for bone substitute biomaterials. We hypothesize that variations in the precipitation conditions will significantly influence the HAp's functional groups, degree of crystallinity, morphology, particle size, and elemental composition. It is also suspected that temperature and time during the synthesis process influence the physical, chemical, and mechanical characteristics of HAp materials. The resulting HA powder was comprehensively characterized using FTIR, XRD, SEM-EDX, PSA, and XRF. The optimized HAp was subsequently used to fabricate a HAp material via the freeze-drying method, followed by evaluation of its compressive strength, pH, and water uptake properties. This research addresses Indonesia's strategic need to develop domestic, sustainable biomedical materials by utilizing abundant local marine resources, thereby reducing reliance on imported bone substitutes.

■ EXPERIMENTAL SECTION

Materials

The chemicals and solvents components, include: NH_4OH (25%, Merck, Germany), H_3PO_4 (85%, Merck, Germany), H_2O (Merck, Germany), and sodium alginate (Merck, Germany) were provided from Merck. Raw material such as gonggong snail shell powder (*S. canurium*) was obtained from Bintan Island, Indonesia.

Instrumentation

The concentration of each particle size was examined using XRF (Epsilon 4 Benchtop XRF analyzer). The particle size of HAp was measured using a PSA Shimadzu SALD-7500 nano. The morphology of HAp was observed using a SEM-EDX (SEM Thermo Scientific Prisma E) and the Fourier transform was examined using the Spectrum Two FTIR with Diamond ATR to study FTIR spectra, (400–4000 cm^{-1}). XRD analysis was performed using a XRD PANalytical Aeris (X-ray Source Copper, Cu) scanned at range of 2θ and the compressive strength of the samples was evaluated using a Shimadzu 5 kN Universal Testing Machine with a crosshead speed of 2 mm/min, initiated at a strain level of 60%.

Procedure

HAp production by wet chemical precipitation

The precipitation synthesis method begins with gonggong snail shell powder calcined in a furnace at 900 °C for 3 h and sieved using a 200 mesh sieve. The snail shell powder is dissolved in distilled water to make

a 1 M $Ca(OH)_2$ solution and stirred for 2 h at 300 rpm using a magnetic stirrer until the $Ca(OH)_2$ is homogeneous. In the calcination and wet chemical precipitation process, the $Ca(OH)_2$ solution is given the addition of 0.6 M H_3PO_4 solution (15–20 drops/min) with stirring at room temperature with a magnetic stirrer at 300 rpm. The next stage is the adjustment at pH 8 by adding NH_4OH solution for up to 2 h. The solution is stirred and left to stand, then allowed to settle for up to 24 h until a white precipitate appears. The final stage is the solution is filtered and rinsed with distilled water, and heated in a furnace with variations in temperature and time, namely 800, 900, and 1000 °C for 4 h and sieved with a 200 mesh sieve [11]. HAp characterization was carried out using various techniques, namely XRF, PSA, SEM-EDX, FTIR, and XRD.

HAp materials fabrication by freeze drying

HAp materials fabrication was performed based on the optimal characterization results obtained from precipitation synthesis at 900 °C for 4 h (HAPT2, see Table 1). The process involved mixing alginate with 200 mL of distilled water using a homogenizer at 10,000 rpm for 5 min, followed by the addition and subsequent 5-min mixing of HAp. The HAp:alginate ratios of 5:5, 7.5:2.5, and 2.5:7.5 (w/w) were employed. The resulting mixtures were cast in 24-well plates, sealed with perforated plastic wrap, and frozen at −80 °C. Lyophilization was then conducted using a freeze dryer at −45 °C and 0.099 mBar for 3 d. The fabricated HAp Materials underwent testing for compressive strength, pH, and water uptake.

■ RESULTS AND DISCUSSION

XRF Characterization of HAp

XRF characterization was performed to identify the chemical composition of gonggong snail (*S. canarium*) shell powder before synthesis and the HAp obtained through precipitation. The XRF results, presented in Table 2, indicate that gonggong snail shells are a promising precursor for HAp synthesis due to their high calcium (Ca) content of 67.70%. The analysis also confirmed the presence of several minor elemental impurities derived from the calcined powder and HAp, including Si, S, Cl, Fe, Sn, Te, Zr, and Mn. Following the precipitation synthesis process with heating at 1000, 900, and 800 °C for 4 h, the resulting Ca/P ratios were 3.181, 2.761, and 3.025, respectively. Notably, the Ca/P ratio closest to the stoichiometric value of HAp (1.67) was 2.76, achieved at a synthesis temperature of 900 °C for 4 h. It is known that HAp derived from natural sources often exhibits non-stoichiometric properties, typically displaying deficiencies in calcium or phosphorus [12]. The observed Ca/P ratios exceeding 1.67 can be attributed

Table 1. Sample codes for gonggong snail shell powder and HAp

Sample name	Code
Untreated powder	BR
Calcined powder 900 °C, 3 h	BF
HA precipitation at 1000 °C, 4 h	HAPT1
HA precipitation at 900 °C, 4 h	HAPT2
HA precipitation at 800 °C, 4 h	HAPT3

Table 2. XRF data for calcined powder and HAp

Component	Calcined powder 900 °C, 3 h (BF) (%)	HAp 1000 °C, 4 h (HAPT1) (%)	HAp 900 °C, 4 h (HAPT2) (%)	HAp 800 °C, 4 h (HAPT3) (%)
Ca	67.69900	43.11300	38.72600	35.00800
P	0.99000	13.55300	14.02600	11.57200
Si	0.00524	0.17500	0.19600	0.14900
S	0.05189	0.04068	0.02567	0.02012
Cl	0.03445	0.00804	0.00399	0.01073
Fe	0.03345	0.02275	0.02308	0.02110
Sn	0.01656	0.01566	0.01582	0.01268
Te	0.00737	0.00655	0.00709	0.00503
Zr	0.00232	0.00166	0.00146	0.00122
Mn	0.00149	0.00103	0.00091	0.00083

to the incorporation of ions such as carbonate into the HAp structure [13] and the presence of trace elements like Mg, Na, Sr, Fe, Al, and Zn, which have been reported to potentially accelerate and enhance bone [14]. Consistent with our findings, Klinkaewnarong et al. [15] reported Ca/P ratios greater than 1.67 in HAp synthesized from limestone using a combination of calcination and precipitation methods, which they attributed to the presence of CaO in the HAp.

PSA Analysis of HAp

Particle size analysis of the gonggong snail shell powder and the synthesized HAp was conducted using a particle size analyzer (PSA). Calcination the shell powder at 900 °C for 3 h (BF) and the subsequent precipitation synthesis of HAp resulted in a reduction in particle size, as shown in Table 3. PSA analysis revealed that the HAp particle size ranged from 1.006 to 1344 μm, with HAp synthesized at 800 °C (HAPT3) exhibiting the smallest particle size (1.006 μm), indicating a trend of increasing particle size with higher precipitation temperatures. This specific combination of heating time and temperature appears more suitable for bone scaffold applications compared to other variations due to the larger surface area it provides, which potentially leads to more effective biological interactions. Smaller particle sizes can contribute to increased particle density and mechanical strength [16]. Furthermore, smaller HAp particles can substantially enhance the efficiency of material absorption, thereby improving product effectiveness and maintaining product stability by extending its shelf life [17].

SEM and EDX Analysis for HAp

SEM instrument was employed to investigate the morphology and microstructure of both the gonggong snail shell powder and the synthesized HAp in Fig. 1. SEM images at 10,000× magnification revealed the presence of agglomerated particles in all samples. Furthermore, some HAp particles exhibited a spherical

Table 3. PSA data for calcined powder and HAp

Sample Name	Particle Size (μm)
BR	8.553 ± 0.627
BF	4.751 ± 0.532
HAPT1	1.236 ± 0.460
HAPT2	1.344 ± 0.426
HAPT3	1.006 ± 0.467

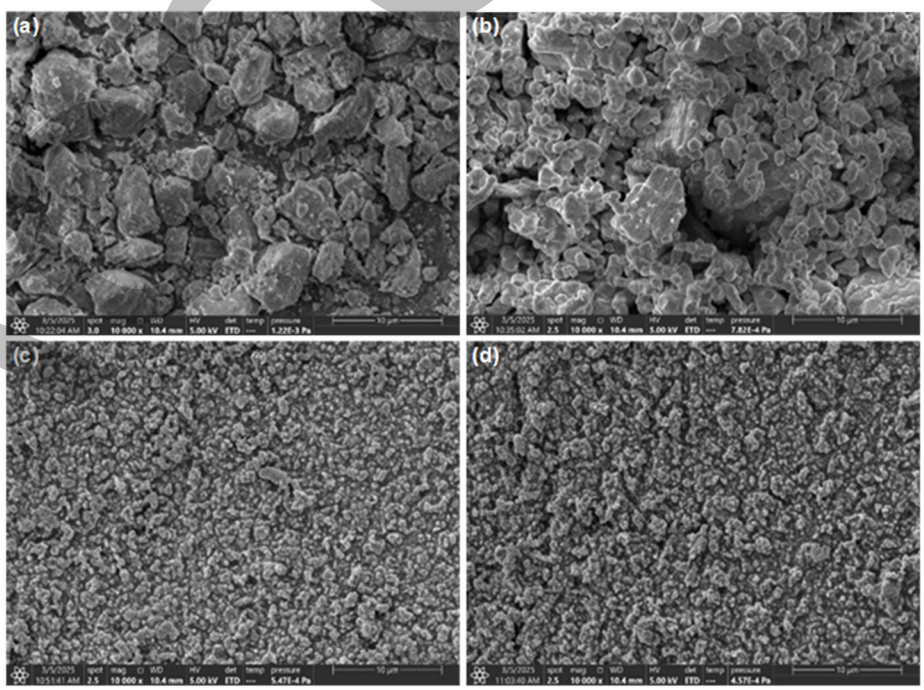

Fig 1. SEM analysis of (a) BF, (b) HPT1, (c) HPT2, and (d) HPT3 in magnitude of 10.000×

shape with a tendency to form irregular granular structures. This granular morphology likely arises from the Ostwald ripening process, where larger calcium phosphate crystals incorporate smaller surrounding crystals [18]. The elevated temperature during the precipitation synthesis influenced the resulting HAp morphology, as HAp is known to reach its agglomeration point around 750 °C. This observation is consistent with our particle size analysis using PSA, which indicated increased particle aggregation at higher synthesis temperatures. The synthesized HAp exhibited small and irregular pore sizes, potentially due to the accumulation of other substances during the process. This inherent porosity in HAp is crucial for providing a favorable biological environment that supports cell adhesion, cell-cell interaction, proliferation, and migration [19]. The pore size of HAp is expected to facilitate new bone tissue growth after implantation. The observed HAp particle agglomeration aligns with the findings of Tourbin et al. [20], who also reported agglomerated HAp particles in their SEM analysis.

EDX analysis was conducted to determine the elemental percentages of Ca and P in the gonggong snail shell powder and the synthesized HAp. The Ca content in the calcined shell powder (BF) was 97.03%. In contrast, the Ca content in the synthesized HAPT1, HAPT2, and HAPT3 was 60.43, 70.92, and 67.17%, respectively. Additionally, EDX analysis quantified the P content in the synthesized HAp samples as 24.91, 29.08, and 32.47% for HAPT1, HAPT2, and HAPT3, respectively. These results suggest that gonggong snail shells are a viable raw material for HAp production due to their high $CaCO_3$ content, which serves as an effective Ca precursor in the synthesis of calcium phosphate. Calcium phosphate derived from biomaterials typically exhibits a Ca/P ratio ranging from 0.5 to 2.0 [21-22].

FTIR Spectra of HAp

FTIR spectroscopy was performed to identify the functional groups present in the gonggong snail shell powder and the synthesized HAp, as depicted in Fig. 2. The FTIR spectra revealed the characteristic functional groups of PO_4^{3-} and OH^-. Specifically, the presence of PO_4^{3-} was indicated by absorption bands at wavenumbers

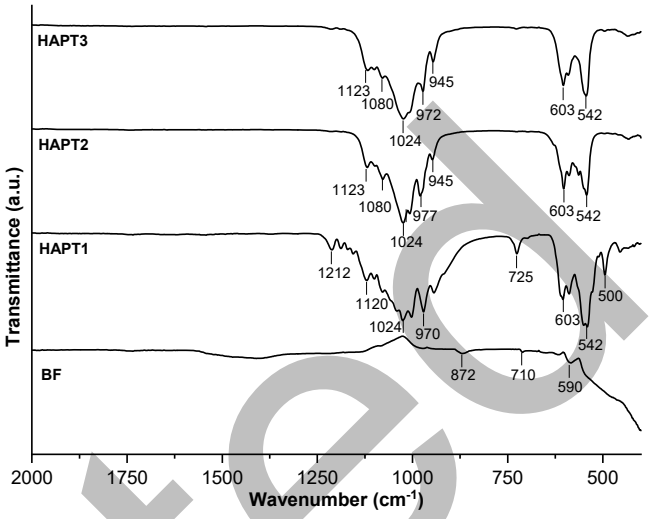

Fig 2. FTIR spectra of calcined powder and HAp materials

1080, 1024, 977, 972, 945, 603, and 542 cm^{-1} in HAPT2 and HAPT3, and at 970, 603, 542, and 500 cm^{-1} in HAPT1. These vibrational wavenumbers for the PO_4^{3-} group are consistent with findings reported by Bano et al. [23], who observed PO_4^{3-} bands in the ranges of 1085–1092, 1033–1035, 1000, 933–962, and 500–611 cm^{-1}. The OH^- functional group was detected in HAPT1 at 725 cm^{-1}, which aligns with the observations of Mondal et al. [24].

XRD Analysis of HAp

The crystalline phases present in the gonggong snail shell powder and the synthesized HAp were identified using XRD. The diffractograms shown in Fig. 3 reveal that the HAPT1, HAPT2, and HAPT3 were predominantly HAp, as confirmed by the Joint Committee on Powder Diffraction Standards (JCPDS) data, card No. 09-0432. This JCPDS card indicates three main characteristic peaks for HAp at 2θ = 31.77°, 32.90°, and 32.19° [25]. The five most intense peaks for HAPT3 were observed at diffraction angles (2θ) of 25.66°, 27.75°, 30.97°, 32.31°, and 34.20°. For HAPT2, these peaks were located at 2θ = 25.66°, 27.75°, 30.97°, 31.70°, and 34.20°, while HAPT1 exhibited its five most intense peaks at 2θ = 27.75°, 29.52°, 30.97°, 32.31°, and 34.20°. The BF in Fig. 3 displayed its most intense peaks at 2θ of 17.94°, 28.63°, 34.11°, 47.14°, and 50.72°. The XRD diffractogram of the calcined snail shell powder indicates

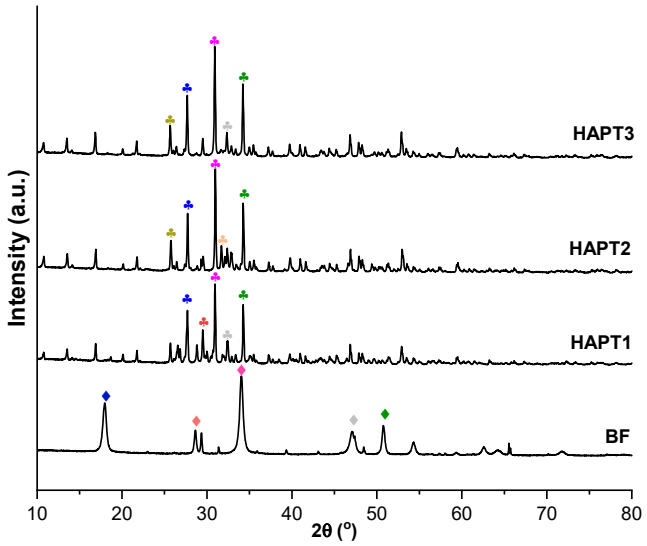

Fig 3. XRD patterns of calcined powder and HAp

a phase transformation from $CaCO_3$ to CaO [26]. This finding is supported by the research of Dahlan et al. [27], who reported the highest intensity peaks for calcined snail shell powder at 2θ = 18.02°, 34.07°, and 50.78°. Furthermore, according to Figueiredo et al. [28], higher sintering temperatures lead to sharper and more defined XRD peaks, which correlate with increased crystallinity.

Compressive Strength of HAp Materials

The mechanical properties of the HAp materials were evaluated through compressive strength tests. These tests were conducted on bone scaffolds (HAPT2) prepared by precipitation synthesis at 900 °C for 4 h. We explored three HAp:alginate (w/w) ratios for these tests: HAPT2A (5:5), HAPT2B (7.5:2.5), and HAPT2C (2.5:7.5). Unfortunately, compressive strength testing was not feasible for HAPT2B samples, as they fractured into powder. This failure stemmed from an insufficient amount of alginate relative to HAp. Given alginate's role as both a matrix and binding agent, a limited composition meant it couldn't effectively integrate the HAp particles or form a strong structural matrix. Consequently, the material became brittle and crumbled. Moreover, a lower molecular weight of alginate would have further exacerbated this issue by reducing chain entanglement and cross-linking, ultimately impairing its mechanical strength [29]. Furthermore, a more limited alginate composition prevented the formation of sufficiently strong cross-linking networks to secure the HAp particles. This also resulted in uneven dispersion of HAp particles, making them susceptible to damage [30].

Compressive strength tests were conducted using a universal testing machine (UTM) in accordance with ASTM D143 standards, with a crosshead speed of 2 mm/min. The HAPT2A samples had an average diameter of 13.90 ± 0.47 mm and a height of 16.67 ± 0.21 mm. HAPT2C samples measured an average diameter of 14.38 ± 0.37 mm and height of 18.10 ± 0.27 mm. Fig. 4 illustrates that HAPT2C exhibited the highest compressive strength, achieving an average maximum force of 123.32 ± 11.62 N and a maximum stress of 0.75 ± 0.08 MPa. At 60% strain, the average force was 45.40 ± 7.04 N, with a stress of 0.28 ± 0.04 MPa. In contrast, HAPT2A showed an average maximum force of 62.56 ± 9.83 N and a maximum stress of 0.41 ± 0.05 MPa. At 60% strain, the average force for HAPT2A was 21.78 ± 2.64 N, and the stress was 0.14 ± 0.02 MPa. Overall, the mechanical strength of the scaffolds

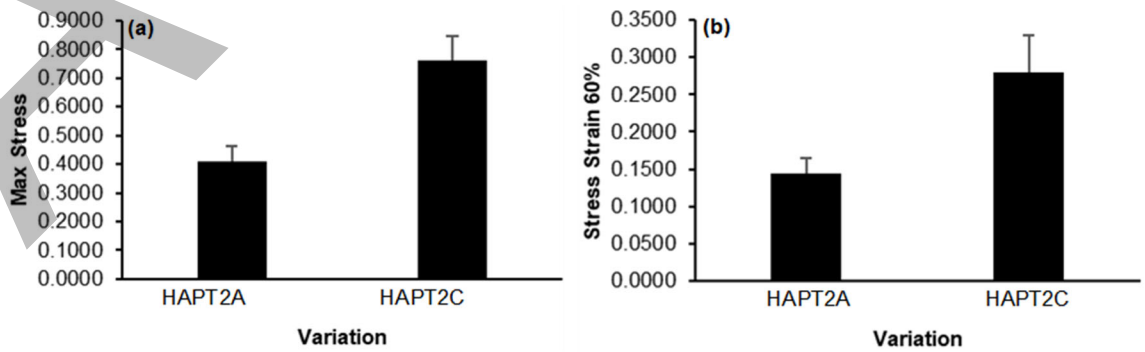

Fig 4. (a) Max stress graph and (b) stress strain 60% graph of HAPT2A and HAPT2C

met the criteria for trabecular bone (0.1–16 MPa) but not for cortical bone (130–200 MP) [31]. Higher mechanical strength in bone scaffolds is a practical advantage because the scaffold functions as a load-bearing support until tissue regeneration is complete [32]. Alginate addition enhances the mechanical properties of bone scaffolds because alginate serves as a polymeric matrix, binding HAp particles to form an interconnected network structure and preventing HAp brittleness [33]. Being a flexible polymer, it contributes to increased fracture toughness and imparts elasticity to the scaffold [34].

pH Test of HAp Materials

pH testing was carried out on precipitation-synthesized (HAPT2A and C), characterized by HAp:alginate (w/w) ratios of 5:5 and 2.5:7.5. The purpose was to ascertain if these HAp-alginate scaffolds leached substances that changed the surrounding pH. Samples were submerged in both distilled water (DW) and simulated body fluid (SBF) for 1, 5, and 10 s. Fig. 5 shows that after immersion, the distilled water's pH reached 10, while the SBF's pH became 8.

The increase in pH to 10 in distilled water was attributed to the release of OH^- ions from HAp. HAp is inherently slightly basic, and upon exposure to deionized water, its surface ions dissociate, raising the concentration of OH^- and consequently the solution's pH [35]. Sutiyono et al. [17] reported that HAp synthesis achieves optimal results within an alkali pH range, where HAp solubility is minimized, and the formation of the desired crystalline phase is most efficient. An alkali pH carries the risk of forming undesirable impurities. However, exceeding pH 12 can lead to excessive incorporation of CO_3^{2-} ions into the HAp structure. A basic environment (pH 8–10) can also promote new bone formation and osteoconduction. The scaffolds immersed in SBF reached a pH of 8, indicating SBF's ability to neutralize the environment by mimicking the ionic composition of human body fluid. This pH stability around 8 in SBF is crucial for biocompatibility, as a near-physiological pH environment (7.4–8.0) supports cell viability and proliferation while minimizing the risk of inflammation.

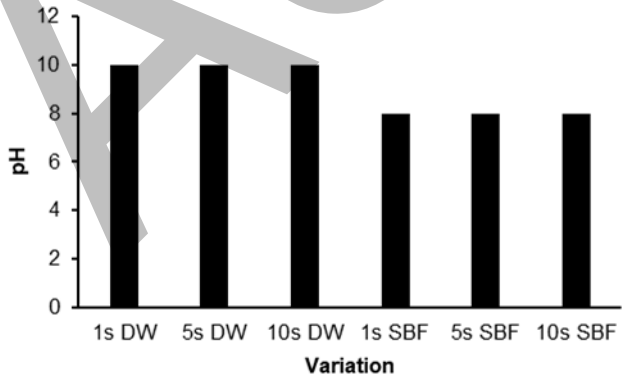

Fig 5. pH Measurement graph in DW and SBF

Water Uptake Test of HAp Materials

Water uptake (WU) was evaluated for HAp materials (HAPT2A and C) at HAp:alginate (w/w) ratios of 5:5 and 2.5:7.5. The objective was to quantify the scaffolds' physiological absorption of fluids and metabolites [32]. Furthermore, the tests aim to quantify the material's ability to absorb bodily fluids and facilitate nutrient exchange [36]. The initial weight of each scaffold was recorded as W0. Samples were then immersed in distilled water and SBF for 1, 5, and 10 s. At the end of each period, the samples were removed from their respective media (DW or SBF), and their weights were recorded. Subsequently, the percentage of water uptake was calculated [37] based on Eq. 1

$$\mathrm{WU}(\%) = \frac{\text{Weight of the sample} - \text{Initial weight}}{\text{Weight of sample}} \times 100\% \quad (1)$$

The WU test results ranged from 556.82 to 747.38% in distilled water and 605.36 to 902.28% in SBF. Specifically, based on Fig. 6(a) that HAPT2A samples exhibited average water uptake values of 747.38 ± 2.50, 577.80 ± 3.17, and 667.12 ± 3.36% for 1, 5, and 10 s variations in distilled water, respectively. In SBF, HAPT2A showed 652.57 ± 1.17, 639.80 ± 2.17, and 796.78 ± 1.72% for the same variations. For HAPT2C based in Fig.6(b), water uptake in distilled water was 710.002 ± 2.80, 676.15 ± 1.33, and 556.82 ± 1.70% for 1, 5, and 10 s variations, respectively. In SBF, HAPT2C exhibited 605.36 ± 4.54, 902.28 ± 2.38, and 765.17 ± 4.90%. Notably, HAPT2A exhibited higher absorption than HAPT2C. This is attributed to the abundant oxygen functional groups in HAPT2A, which promote the formation of hydrogen bonds between the distilled water or SBF and

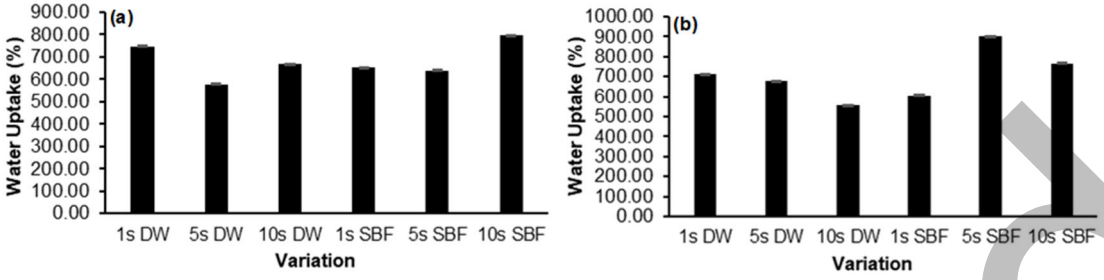

Fig 6. (a) Water uptake graph of (a) HAPT2A and (b) HAPT2C

the bone scaffold [38]. While immersion in SBF is commonly used to simulate *in vivo* conditions for degradation testing, the high-water uptake values primarily indicate the material's high porosity and capacity for fluid transport. The material's final degradation rate and long-term stability will depend on factors beyond water uptake, such as the HAp concentration and the stability of the polymer interface. High concentrations of HAp are known to increase the interface area, which can potentially influence the degradation rate [39].

■ CONCLUSION

The calcium content in gonggong snail shell waste presents a viable raw material for HAp synthesis via precipitation. A Ca/P ratio of 2.76, closely approximating the stoichiometric value of HAp, was achieved through precipitation synthesis followed by calcination at 900 °C for 4 h. PSA revealed that the synthesized HAp particles ranged from 1,006 to 1,344 µm, with the smallest average size (1,006 µm) obtained for HAPT3. SEM results showed that the HAp particles exhibited a non-uniform spherical morphology with a tendency to form granular aggregates. FTIR spectroscopy confirmed the presence of characteristic PO_4^{3-} and OH^- groups. XRD patterns indicated that the HAPT1, HAPT2, and HAPT3 were predominantly the HAp phase, consistent with JCPDS data (card No. 09-0432). The ideal immersion time and temperature for making HAPT2C bone scaffolds (which have a 2.5:7.5 ratio of HAp to alginate by weight), exhibited the highest compressive strength, achieving an average maximum force of 123.3243 ± 11.6211 N and a maximum stress of 0.7599 ± 0.0844 MPa. At 60% strain, the average force was 45.4094 ± 7.0412 N, with a stress of 0.2801 ± 0.0492 MPa. pH test of HAp materials shows that after immersion in distilled water's pH reached 10, while the SBF's pH became 8. The WU test results ranged from 556.82 to 747.38% in distilled water and 605.36 to 902.28% in SBF. HAp from gonggong snail shell are promising biomaterial candidates for bone substitution applications, warranting further investigation through *in vitro* and *in vivo* biocompatibility studies.

■ ACKNOWLEDGMENTS

The authors sincerely thank the National Research Innovation Agency (BRIN). Additionally, thanks are due to Brawijaya University for providing funding and the Faculty of Agricultural Technology for providing knowledge, direction and support during the program. The authors gratefully acknowledge the financial support for this research provided by DRPM Universitas Brawijaya, under the Research Grant Scheme (*Hibah Penelitian*) Number 00738.60/UN10.A0501/B/PT.01.03.2/2025. We express our deepest gratitude for the resources that facilitated the completion of this study.

■ CONFLICT OF INTEREST

The authors have no conflict of interest.

■ AUTHOR CONTRIBUTIONS

Najla Maritza was responsible for conceptualizing and designing the experiment, conducting the experiment, analyzing the data, and writing the paper. Beauty Suestining Diyah Dewanti and Leny Yuliatun were responsible for conceptualization and project administration, providing funding, and revising the paper. The authors actively participated in the discussion of the findings and provided substantial improvements to the final written content.

■ REFERENCES

[1] Firdaus, M.N., Pratista, M.B., Rahman, A., Putera, H.D., and Noor, Z., 2025, The profile of road traffic injury-related fracture patient in the emergency department of H. Damanhuri Barabai general hospital, *J. Orthop. Traumatol. Surabaya*, 14 (1), 37–45.

[2] Kim, T., See, C.W., Li, X., and Zhu, D., 2020, Orthopedic implants and devices for bone fractures and defects: Past, present and perspective, *Eng. Regener.*, 1, 6–18.

[3] Al-Shalawi, F.D., Mohamed Ariff, A.H., Jung, D.W., Mohd Ariffin, M.K.A., Seng Kim, C.L., Brabazon, D., and Al-Osaimi, M.O., 2023, Biomaterials as implants in the orthopedic field for regenerative medicine: Metal versus synthetic polymers, *Polymers*, 15 (12), 2601.

[4] Patil, S., Thanikodi, S., Palaniyappan, S., Giri, J., Hourani, A.O., and Azizi, M., 2025, Sustainable synthesis of marine-derived hydroxyapatite for biomedical applications: A systematic review on extraction methods and bioactivity, *Adv. Manuf.: Polym. Compos. Sci.*, 11 (1), 2508547.

[5] Ramesh, S., Natasha, A.N., Tan, C.Y., Bang, L.T., Niakan, A., Purbolaksono, J., Chandran, H., Ching, C.Y., Ramesh, S., and Teng, W.D., 2015, Characteristics and properties of hydoxyapatite derived by sol–gel and wet chemical precipitation methods, *Ceram. Int.*, 41 (9, Pt. A), 10434–10441.

[6] Kareem, R.O., Bulut, N., and Kaygili, O., 2024, Hydroxyapatite biomaterials: A comprehensive review of their properties, structures, medical applications, and fabrication methods, *J. Chem. Rev.*, 6 (1), 1–26.

[7] Mohd Pu'ad, N.A.S., Koshy, P., Abdullah, H.Z., Idris, M.I., and Lee, T.C., 2019, Syntheses of hydroxyapatite from natural sources, *Heliyon*, 5 (5), e01588.

[8] Naubnome, V., Prihanto, A., Schmahl, W.W., Pusparizkita, Y.M., Ismail, R., Jamari, J., and Bayuseno, A.P., 2025, Chemical precipitation of nanocrystalline hydroxyapatite with calcium carbonate derived from green mussel shell wastes and several phosphorus sources, *Case Stud. Chem. Environ. Eng.*, 11, 101154.

[9] HamidiVadigh, F., and Javadpour, J., 2024, Synthesis of hydroxyapatite nanoparticles using eggshells and two different phosphate sources, *Eur. J. Eng. Technol. Res.*, 9 (2), 1–4.

[10] Gł, M., Kudłacik-Kramarczyk, S., Drabczyk, A., Walter, J., Kordyka, A., Godzierz, M., Bogucki, R., Tyliszczak, B., and Sobczak-Kupiec, A., 2021, Hydroxyapatite obtained via the wet precipitation method and PVP/PVA matrix as components of polymer-ceramic composites for biomedical applications, *Molecules*, 26 (14), 4268.

[11] Ahmed, H.Y., Safwat, N., Shehata, R., Althubaiti, E.H., Kareem, S., Atef, A., Qari, S.H., Aljahani, A.H., Al-Meshal, A.S., Youssef, M., and Sami, R., 2022, Synthesis of natural nano-hydroxyapatite from snail shells and its biological activity: Antimicrobial, antibiofilm, and biocompatibility, *Membranes*, 12 (4), 408.

[12] Gibson, I.R., 2020, "1.3.4A - Natural and Synthetic Hydroxyapatites" in *Biomaterials Science (Fourth Edition)*, Eds. Wagner, W.R., Sakiyama-Elbert, S.E., Zhang, G., and Yaszemski, M.J., Academic Press, Cambridge, MA, US, 307–317.

[13] Sun, R.X., Lv, Y., Niu, Y.R., Zhao, X.H., Cao, D.S., Tang, J., Sun, X.C., and Chen, K.Z., 2017, Physicochemical and biological properties of bovine-derived porous hydroxyapatite/collagen composite and its hydroxyapatite powders, *Ceram. Int.*, 43 (18), 16792–16798.

[14] Doostmohammadi, A., Monshi, A., Fathi, M.H., and Braissant, O., 2011, A comparative physico-chemical study of bioactive glass and bone-derived hydroxyapatite, *Ceram. Int.*, 37 (5), 1601–1607.

[15] Klinkaewnarong, J., and Utara, S., 2018, Ultrasonic-assisted conversion of limestone into needle-like hydroxyapatite nanoparticles, *Ultrason. Sonochem.*, 46, 18–25.

[16] Baye, T.M., and Mekonone, S.T., 2025, Particle concentration and size effect on mechanical properties of natural-hydroxyapatite reinforced

high-density polyethylene composite, *Polym. Polym. Compos.*, 33, 09673911241313175.

[17] Sutiyono, S., Edahwati, L., Wahyudi, M.R.A., and Rahmah, N.A., 2024, Optimization of nano-hydroxyapatite production from limestone with effect of gelatin concentration and pH in sol-gel synthesis, *IJEISE*, 5 (2), 42–49.

[18] Abdel-Aal, E.A., Dawood, R., Ewais, E.M., Kandeel, W.A., Shemis, M.A., and Abdel-Ghafar, H.M., 2021, Synthesis of agglomerated hydroxyapatite nanospheres with performance as anti-viral material, *Int. J. Mater. Technol. Innovation*, 1, 1–17.

[19] Kang, Q., Wang, W., Wu, S., and Hu, G., 2025, B-doped nano-hydroxyapatite facilitates proliferation and differentiation of osteoblasts, *J. Orthop. Surg. Res.*, 20 (1), 60.

[20] Tourbin, M., Brouillet, F., Galey, B., Rouquet, N., Gras, P., Abi Chebel, N., Grossin, D., and Frances, C., 2020, Agglomeration of stoichiometric hydroxyapatite: Impact on particle size distribution and purity in the precipitation and maturation steps, *Powder Technol.*, 360, 977–988.

[21] Dorozhkin, S.V., 2019, Functionalized calcium orthophosphates ($CaPO_4$) and their biomedical applications, *J. Mater. Chem. B*, 7 (47), 7471–7489.

[22] Fan, J., Schiemer, T., Steinberga, V., Vaska, A., Metlova, A., Sizovs, A., Locs, J., and Klavins, K., 2024, Exploring the impact of calcium phosphate biomaterials on cellular metabolism, *Heliyon*, 10 (22), e39753.

[23] Bano, N., Jikan, S.S., Basri, H., Adzila, S., and Zago, D.M., 2019, XRD and FTIR study of A&B type carbonated hydroxyapatite extracted from bovine bone, *AIP Conf. Proc.*, 2068 (1), 020100.

[24] Mondal, S., Park, S., Choi, J., Vu, T.T.H., Doan, V.H.M., Vo, T.T., Lee, B., and Oh, J., 2023, Hydroxyapatite: A journey from biomaterials to advanced functional materials, *Adv. Colloid Interface Sci.*, 321, 103013.

[25] Joshi, K.J., and Shah, N.M., 2023, Structural, morphological & optical studies of hydroxyapatite microplates synthesized using hydrothermal technique, *Mater. Today: Proc.*, In Press, Corrected Proof.

[26] Karaoui, M., Hsissou, R., Alami, M., and Assouag, M., 2023, Physicochemical characterization of snail shells powder prepared by mechanochemical processes and thermal treatment, *J. Met., Mater. Miner.*, 33 (2), 139–147.

[27] Dahlan, K., Asra, D.Y., and Winata, B.C., 2020, Synthesis of calcium phosphate compound from paddy field snail shells (*Pila ampullacea*) as calcium precursor, *J. Phys.: Conf. Ser.*, 1485 (1), 012021.

[28] Figueiredo, M., Fernando, A., Martins, G., Freitas, J., Judas, F., and Figueiredo, H., 2010, Effect of the calcination temperature on the composition and microstructure of hydroxyapatite derived from human and animal bone, *Ceram. Int.*, 36 (8), 2383–2393.

[29] Qosim, N., Dai, Y., Williams, G.R., and Edirisinghe, M., 2024, Structure, properties, forming, and applications of alginate fibers: A review, *Int. Mater. Rev.*, 69 (5-6), 309–333.

[30] Sahoo, D.R., and Biswal, T., 2021, Alginate and its application to tissue engineering, *SN Appl. Sci.*, 3 (1), 30.

[31] Ryan, E., and Yin, S., 2022, Compressive strength of β-TCP scaffolds fabricated via lithography-based manufacturing for bone tissue engineering, *Ceram. Int.*, 48 (11), 15516–15524.

[32] Liu, M., Dai, L., Shi, H., Xiong, S., and Zhou, C., 2015, *In vitro* evaluation of alginate/halloysite nanotube composite scaffolds for tissue engineering, *Mater. Sci. Eng., C*, 49, 700–712.

[33] Kanasan, N., Adzila, S., Mustaffa, N.A., Sidi, S.M., Rahman, M.N.A., Nasir, N.F., and Gurubaran, P., 2017, The effects of sintering temperature on densification and mechanical properties of hydroxyapatite/sodium alginate biocomposites, *MATEC Web Conf.*, 135, 00063.

[34] Ocando, C., Dinescu, S., Samoila, I., Daniela Ghitulica, C., Cucuruz, A., Costache, M., and Averous, L., 2021, Fabrication and properties of alginate-hydroxyapatite biocomposites as efficient

biomaterials for bone regeneration, *Eur. Polym. J.*, 151, 110444.

[35] Mocanu, A., Cadar, O., Frangopol, P.T., Petean, I., Tomoaia, G., Paltinean, G.A., Racz, C.P., Horovitz, O., and Tomoaia-Cotisel, M., 2021, Ion release from hydroxyapatite and substituted hydroxyapatites in different immersion liquids: *In vitro* experiments and theoretical modelling study, *R. Soc. Open Sci.*, 8 (1), 201785.

[36] de Sousa e Silva, F.M., de Carvalho, R.B.F., Silva, G.C.S., Nunes, L.C.C., and Carvalho, L.F.M., 2024, Analysis of the influence of hydroxyapatite on the morphology and absorption capacity of PHB membranes, *Int. J. Adv. Biotechnol. Res.*, 15, 3–15.

[37] Yazdanian, A., Jahandideh, A., and Hesaraki, S., 2023, The effect of green synthesis of TiO_2 nanoparticles/collagen/HA scaffold in bone regeneration: As an animal study, *Vet. Med. Sci.*, 9 (5), 2342–2351.

[38] Miyajima, H., Touji, H., and Iijima, K., 2021, Hydroxyapatite particles from simulated body fluids with different pH and their effects on mesenchymal stem cells, *Nanomaterials*, 11 (10), 2517.

[39] Jamarun, N., Trycahyani, N.A., Arief, S., Septiani, U., and Sisca, V., 2023, Synthesis of hydroxyapatite-polyethylene glycol with in-situ method using calcium oxide from blood shells (*Anadara granosa*), *Indones. J. Chem.*, 23 (3), 618–626.